

# An optimal waterline approach for studying tidal flat morphological changes using remote sensing data: A case of the northern coast of Vietnam

Si Son Tong<sup>a,b,\*</sup>, Jean Paul Deroin<sup>b</sup>, Thi Lan Pham<sup>c</sup>

<sup>a</sup> Space and Applications Department, University of Science and Technology Ha Noi (USTH), Vietnam Academy of Science and Technology (VAST), 18 Hoang Quoc Viet, Ha Noi, Viet Nam

<sup>b</sup> GEGENAA (EA 3795), FR CNRS 3417 Condorcet, Université de Reims Champagne-Ardenne, 2 esplanade Roland Garros, 51100, Reims, France

<sup>c</sup> Ha Noi University of Mining and Geology, 18 Pho Vien, Bac Tu Liem, Hanoi, Viet Nam

## ARTICLE INFO

### Keywords:

Tidal flats  
Landsat  
Waterlines extraction  
Morphological change  
Gulf of tonkin

## ABSTRACT

Tidal flats on the north coast of Vietnam suffer diurnal tide with a tide range varying between 0.3 m and 3.5 m. Along the 350 km long coastline, the diversity of environmental conditions induces various tidal flats with different characteristics. This study applies the waterline method for multi-temporal satellite images to build Digital Elevation Models (DEMs) of tidal flats during the last 25 years. 117 Landsat images acquired with TM, ETM+, and OLI have been processed to construct tidal flat DEMs in 1989, 2000, and 2014. Waterlines extracted from single spectral bands (near-infrared [NIR], short wave infrared [SWIR]) or band ratios (normalized difference water index [NDWI], normalized difference vegetation index [NDVI], Green/SWIR) of the Landsat data have been compared with waterlines digitalized on Spot, Aster and Worldview 2 images. This experiment allows us to determine the best band (or band ratio) for extracting waterlines depending on local conditions. Consequently, the study shows that the Green/SWIR ratio image is a good solution for extracting waterlines in the black coal tidal flats of Cam Pha. However, the NDWI index appears to be a better choice for the other parts of the study area. The vertical accuracy of the tidal flat DEMs reaches 0.144 m. The change analysis of the DEMs also emphasizes the tidal flat evolution in both vertical and horizontal dimensions, i.e. erosion or accretion. The erosion of the tidal flats along the northern coast of Vietnam is particularly developed in the area extending from Yen Hung to Mong Cai, especially in Mong Cai with an amount of about  $50 \times 10^6 \text{ m}^3$  of sediments lost between 1989 and 2014. On the contrary, the tidal flats in the south of the study area show a high rate of deposition due to the sediments fed by Red and Thai Binh rivers. About  $35 \times 10^6 \text{ m}^3$  of sediments deposited in the tidal flat surrounding the Red River mouth between 1989 and 2014. This study represents a development of the waterline extraction method to investigate the evolution of tidal flat at a large scale and a diversified coastal environment using optical satellite images and fieldwork.

## 1. Introduction

The interactions between land, freshwater, and marine environment lead to tidal flats, which are regularly submitted to flooding by the tide (Klein, 1985; Jackson and Bates, 1997; Mackinnon et al., 2012). In general, tidal flats are coastal wetlands, soft-sediment habitats, and they are found along the coasts all over the world with various scales. Vast tidal flats are observed for example in the Mont Saint-Michel bay (Deroin and Shimada, 2010), in the Baie des Veys, France (Deroin, 2012) or the Gomso bay in South Korea (Ryu et al., 2008) or Jiangsu coast of China (Wang et al., 2019). Narrow tidal flats (several meters in width)

are formed surrounding the Arctic coast of Canada or Greenland (Flemming, 2002). The comprehensive knowledge of tidal flats and their changes plays a crucial role in coastal ecology, sediment transport, coastal protection, and coastal management. Still, this information remains limited in most coastal areas (Murray et al., 2012; Kang et al., 2017; Tseng et al., 2017).

Monitoring morphological changes of tidal flats is a big challenge due to short exposure time to the air as well as soft ground to be reached in the field. Thus, only the remote sensing technique with the advantages of rapidly collecting information of objects, multi spatial, multi-temporal, multispectral resolutions allows instantaneously mapping

\* Corresponding author. Space and Applications Department, University of Science and Technology Ha Noi (USTH), Vietnam Academy of Science and Technology (VAST), 18 Hoang Quoc Viet, Ha Noi, Viet Nam.

E-mail address: [tongsison@gmail.com](mailto:tongsison@gmail.com) (S.S. Tong).

<https://doi.org/10.1016/j.ecss.2020.106613>

Received 9 July 2018; Received in revised form 13 January 2020; Accepted 19 January 2020

Available online 22 January 2020

0272-7714/© 2020 Elsevier Ltd. All rights reserved.

such an environment (Derooin and Shimada, 2010). It is possible to investigate tidal flat morphology using Light Detection and Ranging (LiDAR) (Mason et al., 2005; Xie et al., 2011; Wang et al., 2019), a pair of airborne optical stereo images (Mason et al., 1995) or a pair of interferometric radar images (Mason et al., 1995; Won and Kim, 2003). The waterline method is probably the most popular (Koopmans and Wang, 1994; Mason et al., 1997; Lee et al., 2001; Guariglia et al., 2006; Bell et al., 2016; Xu et al., 2016; Kang et al., 2017). Although LiDAR represents a modern airborne remote sensing technique with extremely high accuracy (centimeter-level), it is a high cost when applied in a small area. It is difficult to obtain a synchronized Digital Elevation Model (DEM) over a field under changing tidal conditions such as tidal flats (Kang et al., 2017). Using Interferometric Synthetic Aperture Radar (InSAR) to construct tidal flat DEMs usually produces poor vertical accuracy (meter level) because of the low-coherence interferometry in a wet environment (Mason et al., 1995; Won and Kim, 2003). The term 'waterline' method was coined by Koopmans and Wang (1994) who used a time series of satellite images acquired at different water levels to construct DEMs in tidal flat areas. This method is currently considered the most effective approach. It has been applied in many tidal flats throughout the world (Koopmans and Wang, 1994; Mason et al., 1997; Ryu et al., 2008; Heygster et al., 2010; Kang et al., 2017; Tseng et al., 2017). However, the previous studies manipulated the waterline method in small stable areas with relatively homogeneous coastal environments. Also, the quantitative estimation of the morphological change of tidal flats has rarely been employed at a scale of several hundred kilometers.

The waterline method for constructing DEMs of tidal flats is based on stacking waterlines extracted on satellite images acquired at different water levels (Koopmans and Wang, 1994). One of the most critical features to successfully apply the waterline method is determining an appropriate band or band ratio of satellite images to precisely extract waterlines for a coastal environment. Various spectral bands or band ratios have been used in waterline extraction for many coastal regions throughout the world. The band ratios of spectral reflectance at wavelengths 0.630  $\mu\text{m}$ , 0.695  $\mu\text{m}$ , 0.76  $\mu\text{m}$  were used in Holderness Coast, eastern England (Lohani and Mason, 1999), the Normalized Difference Water Index (NDWI) in East Asia coast (Murray et al., 2012), the middle infrared (MIR) band in the Kyongki bay, South Korea (Lee et al., 2001; Lee and Kim, 2004), the band ratio of red and near-infrared (NIR) in western James Bay and Hudson Bay, Ontario, Canada (Bhargava and Mariam, 1991), the band ratio green/MIR in the Ionian coast, Basilicata, Southern Italy (Guariglia et al., 2006), the band ratios green/NIR and green/MIR in the Persian Gulf (Niya et al., 2013). Previous studies indicated that the accuracy of waterline extraction profoundly depends on the band or band ratios used in a specific coastal environment. However, the suitability of using them for a particular tidal flat has not always been proved. Moreover, even though applying the waterline method on a large scale, these studies used only one threshold value of the selected band to extract the waterlines. This approach affects the accuracy of DEM constructed by the waterline method due to the rapid temporal and spatial variation of a tidal flat environment.

The objective of this study is to identify an optimal approach for waterline extraction in a complex coastal environment with a rapid morphological change of tidal flats on a large scale. Carrying out the waterline method targeted on the non-vegetated tidal flats, we attempt to characterize the tidal flat morphology corresponding to the local tide regime as well as to figure out the tidal flat change related to the extreme tropical cyclones. The case study is located along the northern coast of Vietnam, where tidal flats suffer both erosion and deposition. However, previous studies investigated the increase or the reduction of tidal flats using historical maps or remote sensing techniques (Nguyen, 1996; Tran et al., 2003; Nguyen et al., 2013; Tong et al., 2014). The detailed morphological information and the change of tidal flats remain unknown. Moreover, global DEMs with spatial resolution varying from 30 m to 90 m are missing data in the tidal flat areas. The main current

global DEMs are the Shuttle Radar Topography Mission (SRTM), Advanced Spaceborne Thermal Emission and Reflectance Radiometer Global Digital Elevation Model (ASTER GDEM), Advanced Land Observing Satellite Global Digital Surface Model (ALOS World 3D), TerraSAR-X add-on for Digital Elevation Measurement (TanDEM-X). This study fills the gap of topographic data that plays a crucial role in coastal conservation as well as for coastal planning.

## 2. Study area

The study area is elongated over 350 km along the north coast of the Gulf of Tonkin, Vietnam (Fig. 1). This area suffers the subtropical climate, characterized by the monsoon. The tide corresponds to a diurnal regime with an average of 3.5 m in range. High mountain terrain along with extreme precipitation in rainy season in the northern part (from Hoanh Bo to Mong Cai) form numerous short, steep slope reliefs associated with temporary rivers. Besides, more than 2,300 rocky islands protect coastal zones from the influences of wind and waves. The high dynamics of the hydrology, terrain, and meteorological characteristics, together with the tidal influence, leads to extensive sandy tidal flats. As an example of tidal flats constituted by human activities, the coastal area in Cam Pha in the middle of the study area has been accumulated sediments from coal mines for more than a century. Coal sediments concentrate on near-shore water and form black clay tidal flats. Tidal flats in the area from Kim Son to Yen Hung are fed by a massive amount of sediments from the Red River and Thai Binh River systems. Each year, this river transports an average of about  $77 \times 10^6$  tons of deposits to the coastal area (Hoa, 2001). Notably, the Red River system forms a large estuarine tidal flat, which is prevented by seaward sandbars. The diversity of coastal environments causes difficulties in accurately extracting waterlines on satellite images. In addition, the variation of suspended sediments in the near-shore waters over time and space significantly alters the accuracy of the waterline detection on satellite images.

The study area is divided into 13 coastal sections at relatively equal distances and respecting the administrative borders (Fig. 1). In each coastal section, a cross-section is located on the tidal flat for morphological analysis (red dash lines in Fig. 1). The topographic elevation in Fig. 1 is generated from the SRTM DEM with the range from 5 m to 1800 m. Tidal flats in the surrounding area of the Red River mouths are typically 5 km in width, but they are only hundreds of meters wide in the rocky coastal area in Ha Long, Cam Pha, or Van Don. The extent of tidal flats shown in the map is the area extracted on satellite images, which were acquired at the lowest and the highest tides. Thus it is mentioned as the boundary of tidal flats in this study.

## 3. Data and methodology

### 3.1. Data in use

#### 3.1.1. Satellite images

Satellite images provide the waterlines at different water levels for constructing DEM of tidal flats. A mount of 305 Landsat images captured in 1988–1989, 2000–2001, and 2013–2014 have been pre-investigated to check their usability according to the following criteria: cloud cover, water level, and sea wind speed. We recognized that the estimation of water level usually occurs with low accuracy in the first quarter or the third quarter of the lunar cycle. In these periods, the tidal range between high tide and low tide reaches the minimum, the profiles of water level are not in the typical shape (sine-shaped) that cause the inaccuracy of the tide estimation. Also, images acquired with a sea wind speed higher than 10 m/s force the waterlines far from their locations at the corresponding tidal levels (Sea wind data at 10 m altitude provided by the National Oceanic and Atmospheric Administration (NOAA)). Therefore, the images captured in the above cases are excluded from the database to construct DEMs of tidal flats.

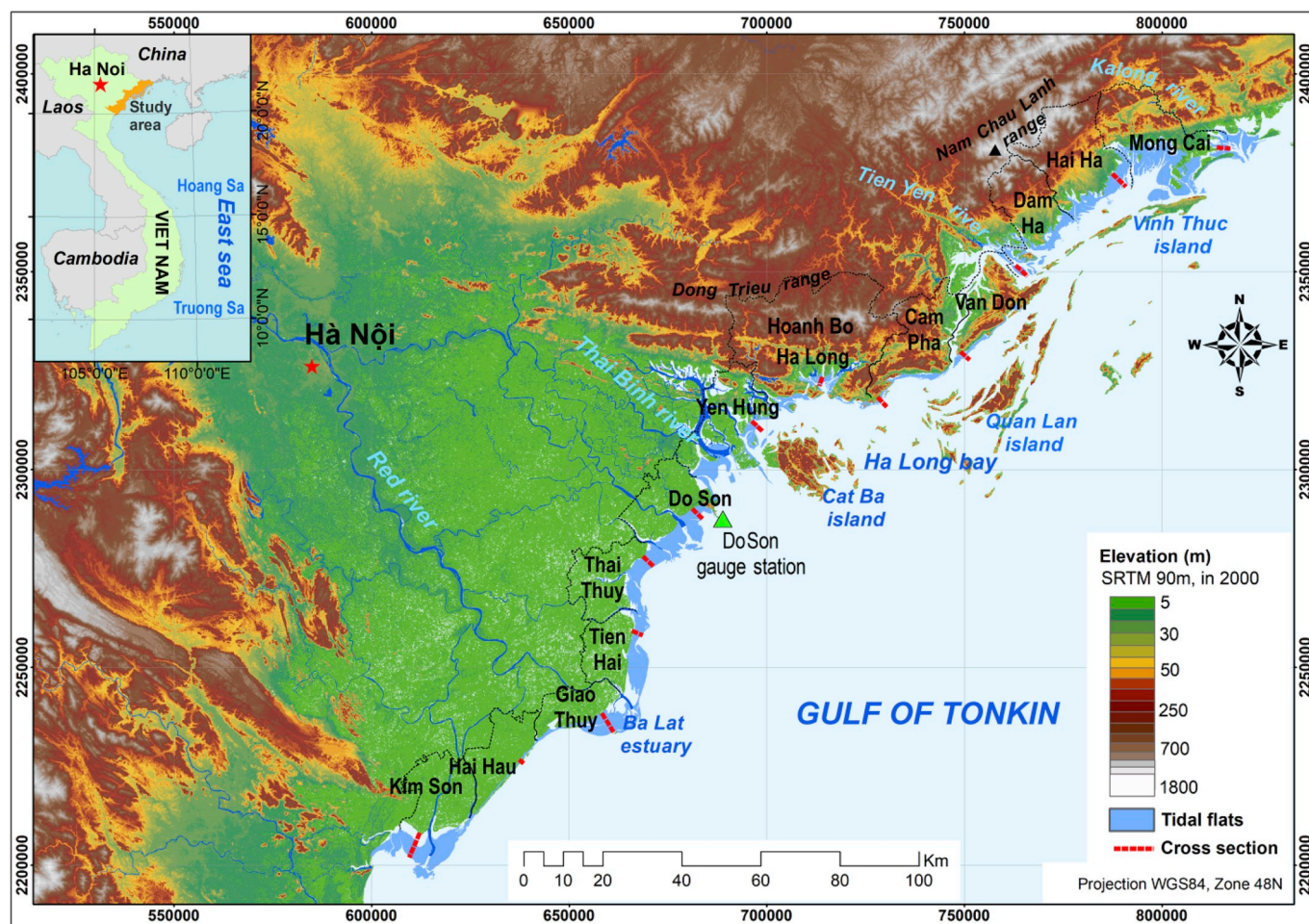


Fig. 1. Map of the study area, including studied tidal flats, surrounding topography, names of coastal sections and the location of the Do Son gauge station (green triangle). (For interpretation of the references to color in this figure legend, the reader is referred to the Web version of this article.)

Consequently, only 117 images have been selected corresponding to the path/row 126/046, 126/045, and 125/045 of Landsat 5 TM, Landsat 7 ETM+, and Landsat 8 OLI. There have been 38 images acquired in 2013–2014, 34 images in 2000–2001, and 45 images in 1988–1989, respectively (Fig. 2). Several Landsat 7 ETM+ images acquired after May 2003 have the Scan Line Corrector error (SLC-off). However, this error is negligible because the non-data strips are just 3 pixels in width, and they are perpendicular to the coastline in the study areas. The dash waterlines caused by this error can be interpolated from non-error area to be solid waterlines. The archived images are processed as Landsat Surface Reflectance High-Level Data products (level L1T) by the United States Geological Survey (USGS). The atmospheric and topographic effects are minimized in these images (Department of the Interior, 2016). All images are systematically spatial co-registered with the root mean square error (RMSE) less than 12m, and they are adjusted to 30 m spatial resolution (pixel size is 30 m × 30 m) in the Universal Transverse Mercator (UTM) projection zone 48N (Zanter, 2017).

Three pairs of satellite images captured on the same day with similar water levels are collected to determine the spectral bands or band ratios for extracting waterlines. Images in each pair overlay each other, and they comprise a Landsat image and a higher resolution image acquired either by EO-Aster, Spot 2, or Worldview 2 sensor (Table 1). The two images of Worldview 2 and Landsat 7 were acquired on the 13<sup>th</sup> April 2015, with a time difference of 37 min corresponding to 2 cm of water level difference. These images cover the coal tidal flats in Ha Long and Cam Pha in the rainy season. The tidal flats, as well as near-shore shallow water, appear black so that it is difficult to determine the

waterlines using the visible bands of satellite images. The pair composed of Spot 2 and Landsat 7 images were acquired on the 31<sup>st</sup> August 2002 with the same highest water level (2.42 m) of the day. They overlay each other 70 km of coastal length from Hai Hau to Giao Thuy in the middle of the area of interest. These images are compared to assess the ability to extract waterlines at high tide in the summertime. The pair composed of Aster and Landsat 7 was acquired on the 17<sup>th</sup> February 2001 with 8 cm different water levels. They cover the area from Kim Son to Thai Thuy along 130 km of the coastline. These images were acquired during the dry season with the lowest suspended sediment content in the near-shore shallow waters. However, the turbidity is greatly varying in the river mouth areas and other locations along the coast. The Landsat image and the higher resolution image of each pair are referred to as the testing image and the reference image, respectively, in the next processes.

### 3.1.2. Water level

The water level provides referent elevation for DEMs by assigning water levels to corresponding waterlines extracted on satellite images. In this study, the water level is real-time estimated from the hydrological models of the Service Hydrographique et Océanographique de la Marine, France (SHOM). This model combines the inaction method and least square estimation into harmonic analysis to predict sea water level at more than 1000 port sites around the world (<https://maree.shom.fr>). The Hondau port in Do Son located in the middle of the study area at 20°40'6.53"N, 106°48'53.50"E is the site of estimating water levels for this study. Generally, water levels are estimated with an accuracy of 3

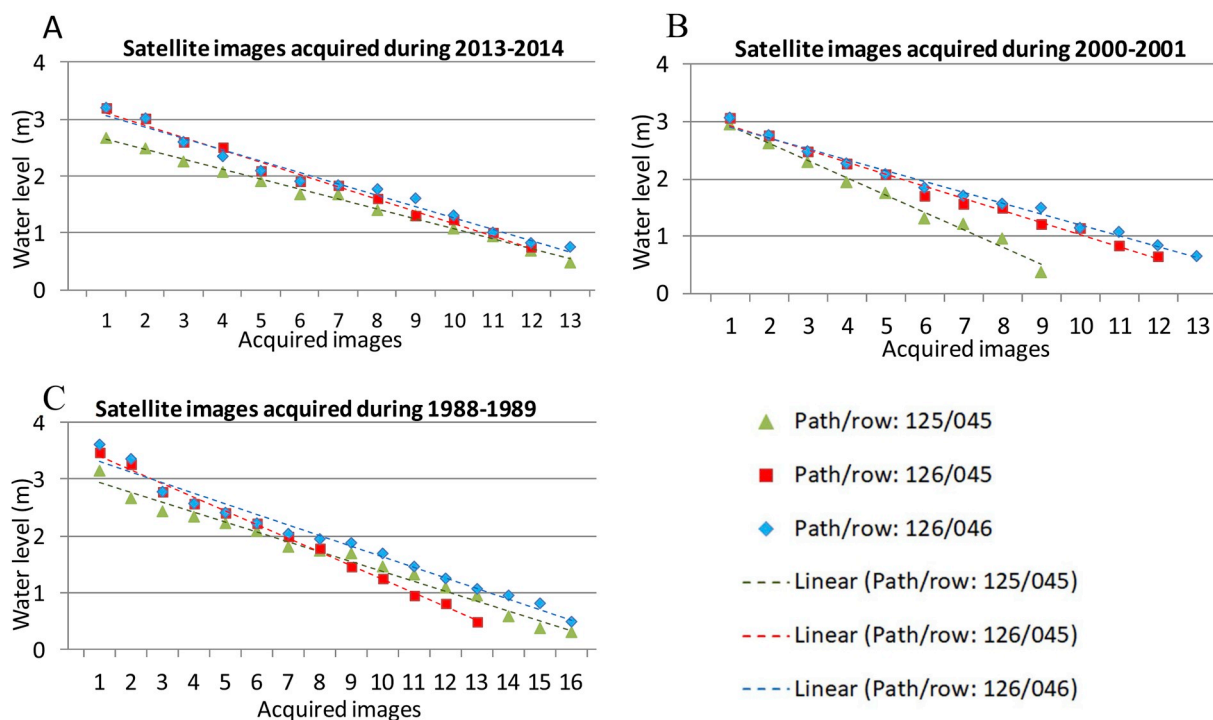


Fig. 2. Water levels corresponding to the order of satellite images acquired on each period (A) 2013–2014, (B) 2000–2001, (C) 1988–1989.

Table 1

Pairs of testing-reference satellite images captured in the same day used to define a solution for extracting waterlines.

Date	Sensor	Path/Row (ID)	Spatial resolution (m)	Acquisition time (UTM)	Water level (m)	Tide state	Coastal areas
13 <sup>th</sup> Apr 2015	Worldview 2	103001003E00BF00	0.5	3:53:00	0.73	Ebb	Cam Pha, Ha Long
	Landsat 7	126/045	30	3:16:26	0.75	Ebb	
31 <sup>st</sup> Aug 2002	Spot 2	271309	20	3:30:25	2.42	Flood	Thai Thuy, Giao Thuy
	Landsat 7	126/046	30	3:05:16	2.42	Flood	
17 <sup>th</sup> Feb 2001	Aster	2150506867–2150506970	15	3:46:19	0.99	Ebb	Kim Son to Do Son
	Landsat 7	126/046	30	3:07:29	1.07	Ebb	

min of time, and 5 cm of elevation of the Lowest Astronomical Tide (LAT). Fig. 2 presents water levels at the acquisition times of Landsat images on each path/row. As an example, a total of 16 satellite images captured at water levels ranging from 0.5 m to 3.2 m produces 16 waterlines with an even elevation distribution of around 0.18 m in the path/row 126/046 (Fig. 2C). The higher density of waterlines achieves better accuracy in constructing DEMs. Moreover, the even distribution of water levels possibly presents a reliable tidal flat if its topography is previously unknown, and a limited number of waterlines are usable to construct DEMs.

### 3.1.3. In situ data

Fieldworks allow us analyzing sediment types, morphologies, also measuring elevation along four transects on the tidal flats in Thai Thuy, Hoanh Bo, Cam Pha, and Hai Ha for accuracy assessment of the DEMs constructed by the waterline method. Elevation profiles of tidal flats were surveyed in July 2015 using Leica TS02plus total station equipment. The equipment measures azimuth angle and distances between the instrument and a reflector to calculate the elevation and horizontal coordinates of monitoring points. Five given parameters: coordinates of control points, the absolute elevation of control points, the height of the instrument, the height of the reflector, horizontal coordinates of starting points are inputs for the survey. The coordinates of control points and starting points are determined in the field using a handheld GPS instrument. The absolute elevation of the first control point is defined as

the elevation of tidal flat DEM 2014 in the middle of each transect. Four rules are respected during the survey: 1/the distances between monitoring points must be around 30m to fit with the Landsat images. 2/the distance between two adjacent control points is 200 m at maximum. 3/backward measuring to previous control point for adjustment. 4/for each transect, the measurement is implemented from the lowest to the higher part of the tidal flat to avoid the influence of flooding tide. The coordinates and elevation of monitoring points are automatically calculated and recorded in memory sticks of the total station equipment.

### 3.2. Methodology

The method to quantify tidal flat change comprises three main steps. 1/First, it is necessary to determine the most appropriate spectral band or band ratio to use for waterline extraction on satellite images. It is important to consider the different environmental conditions (material of tidal flats, the turbidity of shallow coastal water, etc.), which may conduct discrete results in the study area. 2/Second, the waterline method is applied to construct DEMs of tidal flats. 3/Third, the comparison of the DEMs to calculate the sediment budget of tidal flats in 1989, 2000 and 2014 and estimate the gain (or loss).

#### 3.2.1. Extracting waterlines from satellite images

We remain that the Landsat 7 ETM+ bands are B1 (blue range), B2 (green range), B3 (red range), B4 (NIR range), and B5 (MIR range),

respectively. To select an appropriate spectral band or band ratio to extract waterlines on Landsat images, we compare the waterlines derived from ratios B2/B5, NDVI, NDWI, and the single band B4, B5 of the three testing images with reference waterlines visually digitalized on reference images (Table 1). Horizontal profiles of testing images have been firstly investigated the variation from water to tidal flats, as seen in Fig. 3. A threshold to define waterline should be the value at which the profile critically changes. Testing waterlines generated by the thresholds are converted to points with an equal interval of 60m. The ratio or single band image with the smallest Euclidean distances from the points to the corresponding reference waterlines is a suitable option for waterline extraction. The NDWI and NDVI ratios are calculated according to equation  $(B4 - B2)/(B4 + B2)$ , and equation  $(B4 - B3)/(B4 + B3)$  (McFeeters, 1996), respectively. In each testing image, the near-shore shallow water is relatively separated into clear water and turbid water areas to assess the ability of waterline extraction in different turbidities,

as shown in Fig. 3A.

### 3.2.2. Waterline method

The waterline method in this study is composed of the following steps: 1/Extraction of waterlines; 2/Estimation of water level; 3/Assignment of water levels to the associated waterlines; 4/Constructing DEMs using waterlines assigned water level. Waterlines are extracted from 117 Landsat images using thresholds determined on selected band or band ratio. However, using only one threshold to detect waterlines for the whole extent of a Landsat scene does not produce an accurate waterline due to the different turbidity of near-shore water as well as the difference of tidal flats along the coast. Therefore, 13 thresholds are independently determined for 13 coastal sections of the study area. To each extracted waterline is assigned the corresponding water level. All the vertices of these waterlines are used to generate the Triangular Irregular Network (TIN), which presents the surface of terrain as a set of

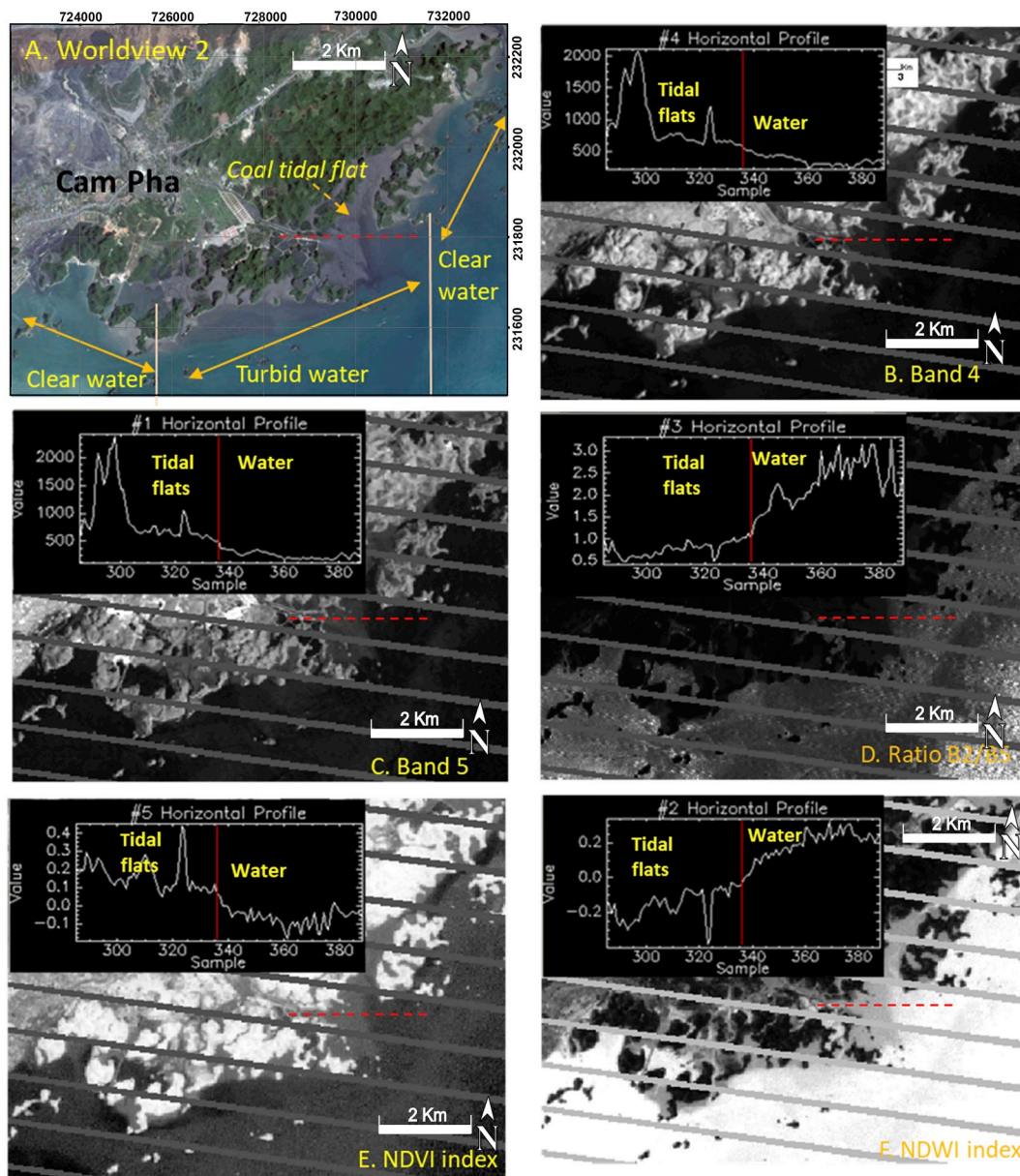


Fig. 3. Testing satellite images captured on the 13<sup>th</sup> April 2015 in Cam Pha (coal tidal flat), (A) Natural color composite of Worldview 2 image with separated turbid water and clear water areas, (B) Band 4 (Near Infrared), (C) Band 5 (Middle Infrared), (D) Ratio B2/B5, (E) NDVI, (F) NDWI images calculated from Landsat 7 ETM+ image with profiles of the cross-section (red dashed line) and threshold (red line) determining water and exposed tidal flats. (For interpretation of the references to color in this figure legend, the reader is referred to the Web version of this article.)

contiguous, non-overlapping triangles. A DEM is generated by converting the TIN model using the natural neighbor interpolation algorithm (Sibson, 1981). Fig. 4 illustrates the procedures of making DEMs from waterlines. In this study, three DEMs constructed in 1988–1989, 2000–2001, 2013–2014, so-called DEM 1989, DEM 2000 and DEM 2014, respectively, are resized to the pixel size of 30 m in the WGS 84 zone N48 projection. The later DEM is subtracted from the earlier DEM to investigate the change of tidal flats. Negative results illustrate the erosion, whereas positive results correspond to deposition. Vertical variations of tidal flats are multiplied by a pixel size area of DEM (900 m<sup>2</sup>) to estimate the sediment transports in tidal flats for a specific period. Consequently, the mass of sediment loss and sediment concentration due to erosion and deposition is calculated for the 13 coastal sections of the study area.

In sum, an ensemble of the waterline extraction method is developed due to the heterogeneity of tidal flats of the study area. Either a specific band ratio or a spectral index method or a single threshold method is working for all the Landsat images. Thus, to achieve an acceptable DEM production, a combination of band ratio and a spectral index are used, and multiple thresholds are applied for collected Landsat images.

## 4. Results

### 4.1. Identification of an optimal approach for waterline extraction

As shown in Fig. 3, it is not easy to distinguish water from non-water by visual interpretation using the NDVI image in the coal tidal flat near Cam Pha (Fig. 3E). The NDVI values gradually increase from sea to land that causes the difficulty of determining waterlines for both clear water and turbid water. The presentation of the B4 image and NDVI image is almost alike. The NDWI index is the combination of green and near-infrared bands, which are absorbed by black and high moisture surface. Thus it deals with the challenge to distinguish coal tidal flats and the near-shore shallow water in the NDWI image (no significant change at the edge of tidal flat on the profile in Fig. 3F). However, the waterline can be obviously recognized in a clear water area on the NDWI image. The ratio B2/B5 image presents an opposite brightness between water and non-water, the brighter color corresponding to clearer water, more canopy density being a darker color, and tidal flats differing from water and land by the gray areas. This ratio image is the best option comparing to the others because of the dramatic drop of the profile at the position of

waterlines (Fig. 3D). On the other hand, the B2/B5 image has a lot of noise due to very high B5 reflectance of objects as boats surrounding the coast, and it is affected by even thin clouds or water remnants on tidal flats. The MIR radiations (B5) are absorbed by water with more than 2 cm deep, and it strongly reflects on the dry surface (Lee et al., 2001). Accordingly, tidal flats with non-remnant water are clearly determined in the B5 image even with the extremely turbid water.

Euclidean distances between testing waterlines and reference waterlines are represented in Fig. 5. The distance extracted in coal tidal flats in the ratio B2/B5 image of the pair Worldview 2 - Landsat 7 ETM+ reaches the smallest in both clear water (18.3 m) and turbid water (21.2 m) (Fig. 5A). In the pair Spot 2- Landsat 7 ETM+ acquired on 31<sup>st</sup> August 2002 (Fig. 5B), the average distance of the B4 in turbid water (532.7 m) is a hundred times higher than that in clear water (15.4 m); thus it is not shown in the statistic plot. The NDWI represents the highest potential to extract waterlines due to the smallest Euclidean distance in both clear water (12.4 m) and turbid water (15.1 m). Besides, the standard deviation of NDWI is also the lowest with 10.6 m in clear water, which confirms the highest reliability of this index image for determining waterlines. In the dry season (Fig. 5C), NDVI and NDWI images are suitable for extracting waterlines. However, NDWI is better than NDVI since the standard deviation of NDWI is smaller than that of NDVI during ebb tide. Consequently, the Green/MIR ratio image is the best option to extract waterlines in coal tidal flats in Cam Pha, the NDWI index is appropriate for the rest of the study area.

Table 2 contains the average, the standard deviation (Std), and the coefficient of variation (CV) of the thresholds detected on 117 Landsat images following 12 coastal sections using the NDWI index, and Cam Pha section using band ratio green/MIR. These thresholds are grouped into the dry season and the rainy season to observe the influence of seasonal variation on thresholds. In general, the thresholds defined in the dry season are significantly higher than that in the rainy season because of the more upper suspended sediment in near-shore water in the rainy season (Lefebvre et al., 2012). Moreover, CV in the rainy season is extremely high (up to 1231% in Kim Son, 666% in Giao Thuy) that presents the dispersion of thresholds corresponding to the heterogeneity of suspended sediment in near-shore water surrounding estuaries. The coastal area from Kim Son to Do Son gathers all six river mouths of the Red River, which transport a massive amount of alluviums to near-shore water in the rainy season, but almost negligible in the dry season (Nguyen, 2006). Thus, the NDWI thresholds in this area have the

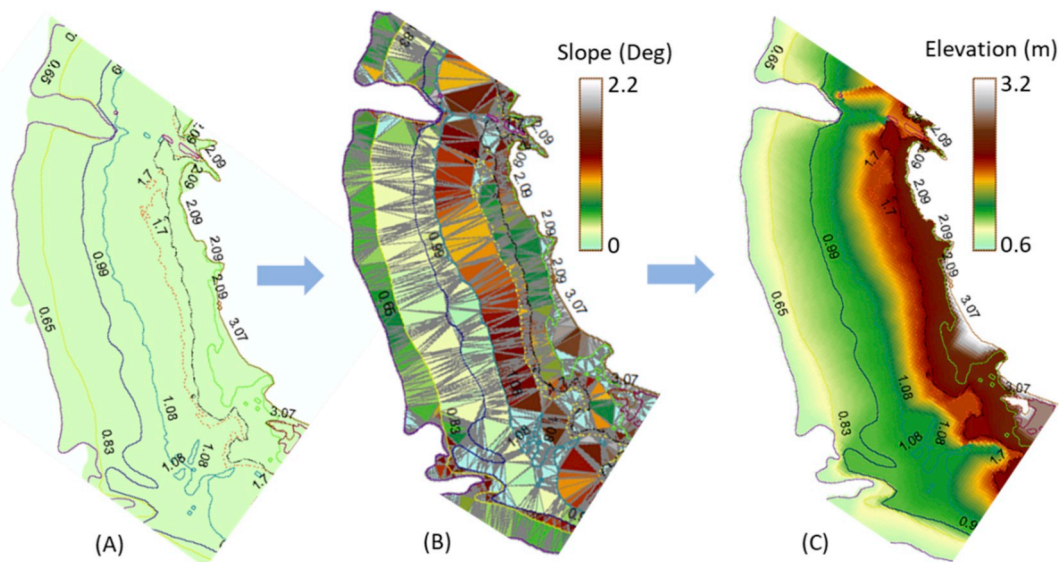


**Fig. 4.** Procedure of making DEM of tidal flats from waterlines, (A) waterlines assigned water levels (m), (B) TIN of tidal flat, the triangles with the same slope presented by the same color, (C) DEM of tidal flat interpolated from the TIN. (For interpretation of the references to color in this figure legend, the reader is referred to the Web version of this article.)

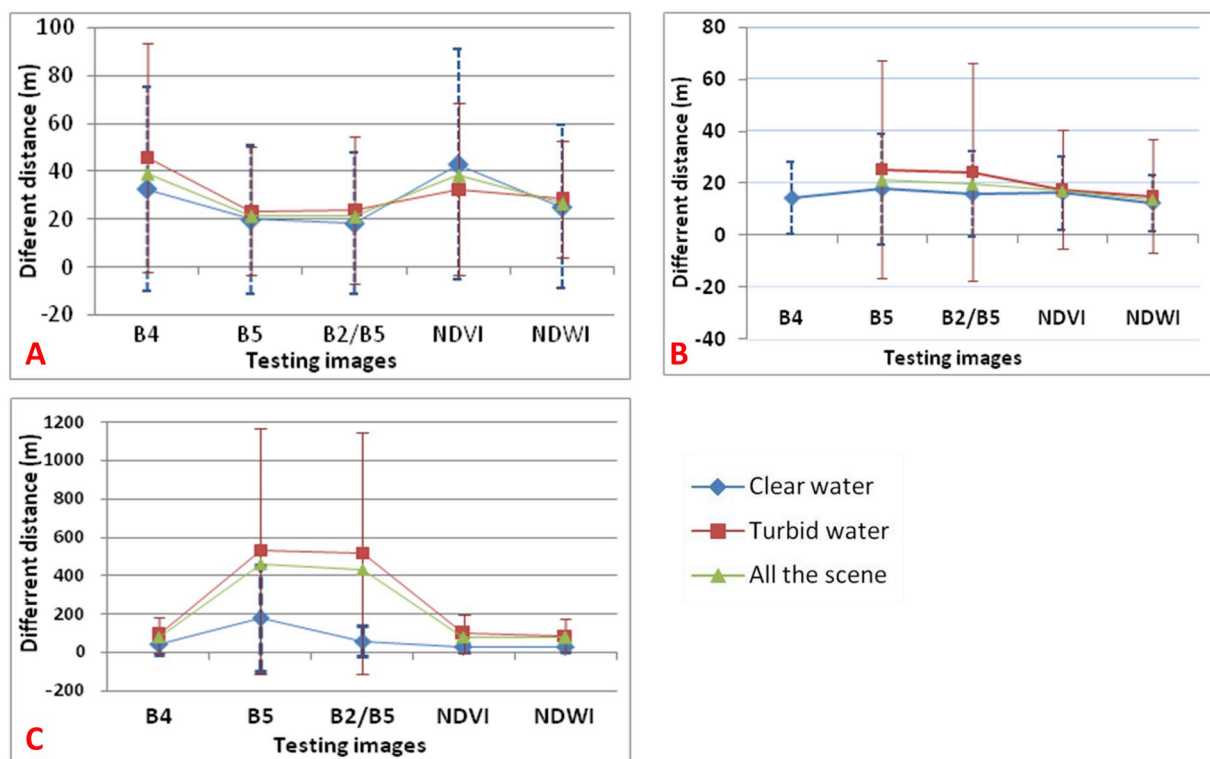


Fig. 5. The plot of Euclidean distance between reference waterlines and testing waterlines of the image pairs captured on (A) 13<sup>th</sup> April 2015, (B) 31<sup>st</sup> August 2002, (C) 17<sup>th</sup> February 2001.

Table 2

Average, standard deviation (Std), and coefficient of variation (CV) of thresholds to extract waterlines in the 13 coastal sections, determined using the green/MIR ratio in Cam Pha and NDWI ratio in the 12 other sections.

Parameter	All the time			Dry season			Rainy season		
	Average	Std	CV%	Average	Std	CV%	Average	Std	CV%
Kim Son	0.031	0.057	187%	0.077	0.017	23%	-0.004	0.051	1231%
Hai Hau	0.025	0.058	235%	0.073	0.018	25%	-0.007	0.057	-814%
Giao Thuy	0.025	0.064	256%	0.071	0.021	30%	-0.010	0.063	666%
Tien Hai	0.024	0.063	263%	0.068	0.021	31%	-0.011	0.070	-636%
Thai Thuy	0.022	0.060	273%	0.067	0.017	25%	-0.011	0.075	-682%
Do Son	0.019	0.056	300%	0.060	0.015	25%	-0.015	0.055	362%
Yen Hung	0.073	0.041	56%	0.128	0.060	47%	0.015	0.027	180%
Hoanh Bo-Ha Long	0.064	0.070	109%	0.137	0.084	61%	0.028	0.014	50%
Cam Pha	1.788	0.478	27%	2.244	0.282	13%	1.560	0.383	25%
Van Don	0.086	0.112	130%	0.191	0.097	51%	0.032	0.036	113%
Dam Ha	0.093	0.125	135%	0.203	0.167	82%	0.037	0.043	115%
Hai Ha	0.049	0.070	142%	0.078	0.087	111%	0.016	0.012	78%
Mong Cai	0.069	0.076	109%	0.096	0.096	100%	0.040	0.027	67%

smallest value in the rainy season (-0.02 in Do Son) due to the very strong reflectance of green wavelength from extremely high suspended sediment in near-shore water. Alternately, the highest threshold (0.09) in Dam Ha denotes the most transparent near-shore water compared with other coastal sections.

Waterlines in Cam Pha are determined in the Green/MIR ratio image with the average thresholds of 2.24 in the dry season and 1.56 in the rainy season. The insignificant change of thresholds between seasons can be explained by the continuous coal exploitation all the time. Moreover, minimal values of the CV (13% in the dry season and 25% in the rainy season) present the appropriateness of using ratio Green/MIR images to extract waterlines in the coal tidal flats. Overall, the distinction of thresholds between the dry season and the rainy season, and between 13 locations along the coast proves that the accuracy of waterline extraction is not only affected by the temporal variation but also the spatial distribution. Therefore, the multiple thresholds

determined in different coastal sections are an efficient solution to maximize the accuracy of waterline extraction due to the heterogeneity of tidal flats in the study area.

#### 4.2. Accuracy assessment of waterline-derived DEM

The elevation of tidal flats measured at four sites in the field in 2015 is used to assess the accuracy of DEM constructed in 2014 using the waterline method. As seen in Fig. 6, the highest accurate DEM is found in Hai Ha with RMSE = 0.072 m and R<sup>2</sup> = 0.981 (Fig. 6C). The accurate DEM in Hai Ha can be explained with three reasons. 1/Shallow near-shore water in Hai Ha is clearer than in other regions so that the waterlines on satellite images are extracted more accurately. 2/Tidal flats in Hai Ha are constituted by coarse particles (Nguyen, 2006), and the ground is solid that minimizes the errors caused by installing equipment and manipulating measurement. 3/Tidal flats are relatively stable (0.18

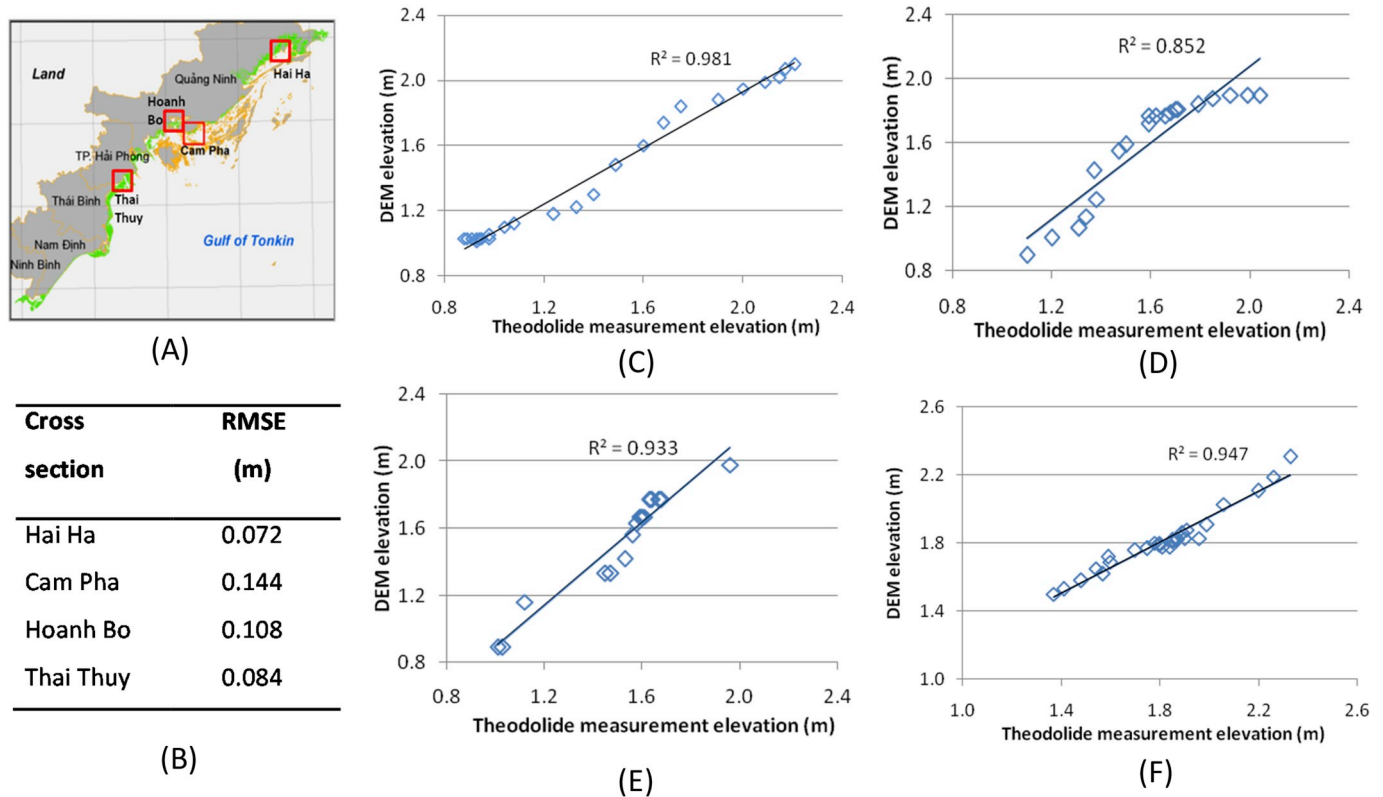


Fig. 6. (A) Locations of field measurement in 2015, (B) RMSE of DEM 2014, comparison of DEM elevation and field measurement elevation of a tidal flat in (C) Hai Ha, (D) Cam Pha, (E) Hoanh Bo, and (F) Thai Thuy.

m of vertical change during the period 2000–2014). The effect of vertical variation during the time scale from the constructing DEM (2014) to the field measurement (2015) is negligible.

Tidal flats in Thai Thuy are similar to those in Hai Ha with a relatively stable ground (insignificant vertical change of 0.116 m in period 2000–2014). However, suspended sediments in near-shore shallow water in Thai Thuy are higher than in Hai Ha (Nguyen, 2006). Thus the accuracy of extracting waterlines in Hai Ha is better than in Thai Thuy. The maximum RMSE is 0.144 m in Cam Pha, where the tidal flat is constituted of coal sediment. The use of ratio green/SWIR image is proved as the best solution for extracting waterlines in Cam Pha, but the black near-shore water along with very muddy soft ground still causes the error of water extraction. Consequently, the vertical accuracy of DEM can be mentioned as the maximum error (0.144 m) in this experiment. The accuracy of estimating the sediment budget is calculated by multiplying the vertical change error and the pixel area of the DEM, which results in  $\pm 259.2 \text{ m}^3$  of sediments.

#### 4.3. The variation of tidal flats

Fig. 7A illustrates the average of 13 elevation profiles extracted along 13 cross-sections on DEM 2014. The horizontal and vertical axes are the lengths and the mean of tidal flat elevation, respectively. It is obviously seen that the profile can be divided into three parts P1, P2, P3, based on the significant change of the altitude. Part 1 is characterized by a steep slope with an elevation ranging from around 1.9 m–3.2 m. Part 2 is ranging from approximately 0.9 m–1.9 m, corresponds to a broad plain. A narrow area located at the lowest part of the tidal flats (part 3) has been measured with an elevation lower than 0.9 m. The three-part separation of tidal flats in Fig. 7A is fitted with the elevation frequency of 13 cross-sections (Fig. 7B) by the significant variations at the elevation marks of 0.9 m and 1.9 m (also known as milestones of 3 parts). Moreover, a logical relation between tidal flat morphology and

tide regime can be observed in Fig. 7C. The range of part 1 fits with the region from the mean tide (1.92 m) to the average of high water spring (HWS) and high water neap (HWN) (2.96 m). The range of part 2 corresponds with water level from the average of low water neap (LWN) and low water spring (LWS) (0.89 m) to the mean tide (1.92 m). Part 3 relates to tidal range from the average of the lowest level of LWS and LWN (0.3 m) to the average of LWN and LWS (0.89 m). Consequently, the tidal flats of the study area are subdivided following the elevation scheme of high tidal flat (1.92 m–2.96 m), middle tidal flats (0.89 m–1.92 m) and low tidal flats (0.30 m–0.89 m) corresponding to Part 1, Part 2 and Part 3. The quantitative change of tidal flat is analyzed in the next steps according to this subdivision scheme.

As illustrated in Fig. 8, the horizontal variation of tidal flats over the years 1989, 2000, and 2014 are quantified according to the three-part scheme, including a small region of supratidal areas. The tidal flats in 1989, 2000 and 2014 cover 76,400 ha, 69,400 ha, and 55,600 ha, respectively. The decrease of the total area does not reflect the erosion because the area of tidal flats depends on the waterlines at the lowest tide, which is not always determined on satellite images. However, the gradual degradation of mid tidal flats from  $38.6 \times 10^3 \text{ ha}$  in 1989 to  $36.7 \times 10^3 \text{ ha}$  in 2000 and  $35.9 \times 10^3 \text{ ha}$  in 2014 proves the erosion over the years. High tidal flats are close to the mainland, hence the critical loss of  $11.9 \times 10^3 \text{ ha}$  from 1989 to 2014 is clearly linked with human activities as projects for mangrove forest development along the coast in Thai Thuy, Giao Thuy and Kim Son (Tong et al., 2014; Pham et al., 2010). Moreover, the recent development of infrastructures contributed to land reclamation in the high tidal flats in Ha Long and Cam Pha (Nguyen, 2006). The horizontal changes of tidal flats indicate the direction of expansion or shrinkage, which is not investigated in the vertical change analysis.

Fig. 9 illustrates the maps of vertical change of tidal flats achieved by subtracting DEM 1989 from DEM 2000 (Fig. 9A), and by subtracting DEM 2000 from DEM 2014 (Fig. 9B). Vertical changes of tidal flats are

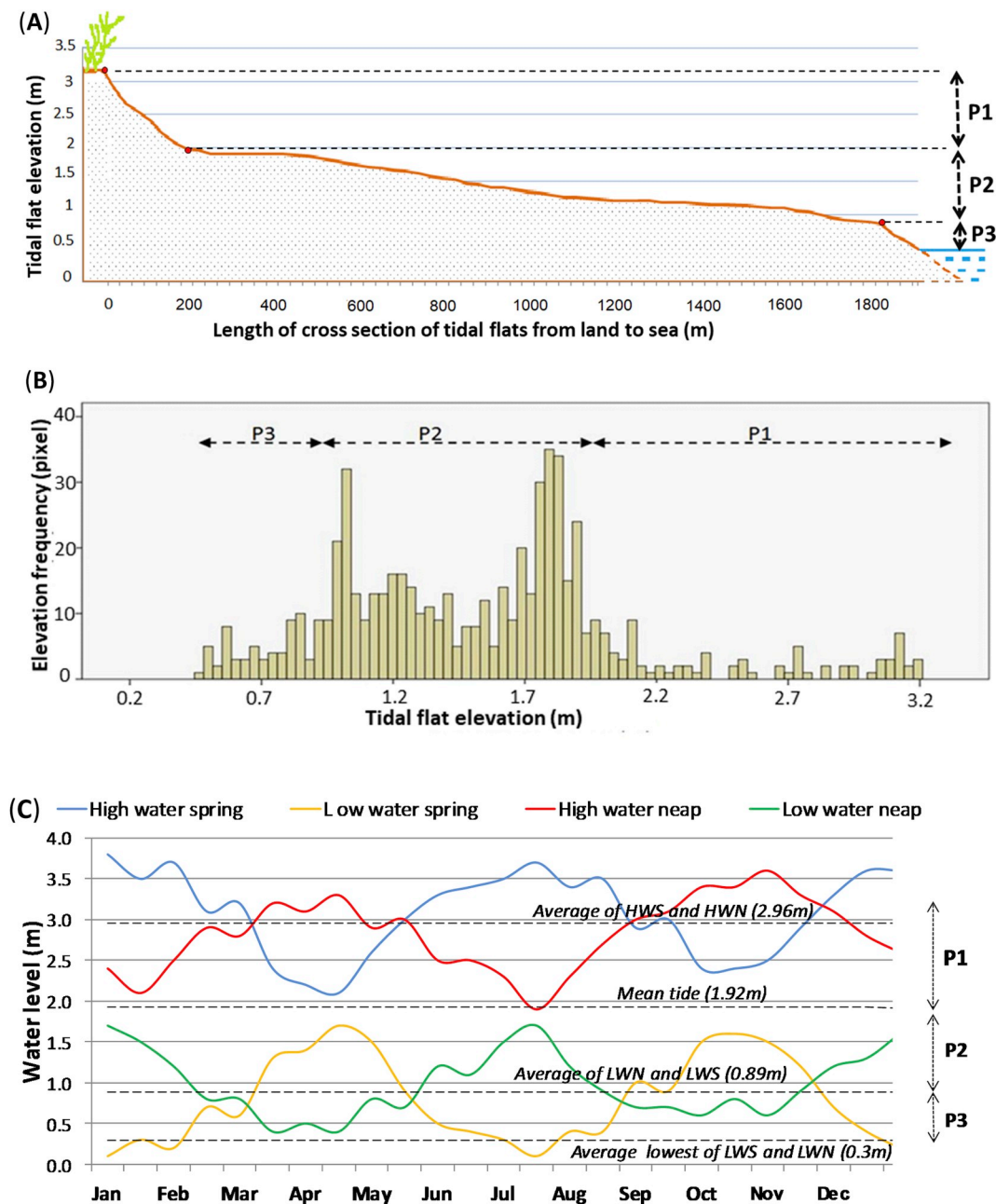


Fig. 7. Subdivision of tidal flats corresponding to (A) Elevation average of 13 tidal flat profiles extracted on DEM 2014, (B) The elevation frequency of tidal flats along 13 profiles, and (C) Tide regime investigated during 2014 in Do Son gauge station.

displayed as the color ramp from red to green, corresponding to the minimum and maximum values of the elevation variation. The critical change of  $-2.65$  m during 1989–2000 represents the dramatic erosion, which appears as narrow strips on the seaward edges of tidal flats surrounding areas of the Red River mouths and Day River mouth. This erosion relates to the movement of sandbars obstructing tidal flats in the estuarine environment (Tong et al., 2014). Simultaneously, significant accretions are found in the center of tidal flats due to the enormous sediment contribution of the rivers. The comparison between two maps generally shows a higher deposition during 2000–2014 rather than during 1989–2000. Alternately, erosion is the predominant trend in Mong Cai and Hai Ha, during periods. The vertical change maps provide reliable data for further estimation of sediment transportation in tidal flats.

The amount of sediment deposition (positive value) and sediment loss (negative value) for each coastal section during 1989–2000 and

2000–2014 is indicated in Table 3. Simultaneously, Fig. 10 illustrates the sediment variation within 25 years from 1989 to 2014 with green columns and red columns corresponding to accretion and erosion. The comparison of sediment import, export represents the magnitude of the deposition or decay, which may coincide in each coastal section. In general, the study area can be divided into deposition and erosion areas. Depositional areas are observed from Kim Son to Yen Hung with a higher amount of sediment concentration than sediment loss. However, the tidal flat in Hai Hau appears as an exception. In this place for both periods 1989–2000 and 2000–2014, the amount of sediment exported is dominating with  $2.6 \times 10^6$  m<sup>3</sup>, and  $1.2 \times 10^6$  m<sup>3</sup>, respectively. Simultaneously, there is only a small amount of deposits accumulated in tidal flats with  $0.6 \times 10^6$  m<sup>3</sup> during 1989–2014. Concurrently, the coast of Hai Hau has suffered severe erosion for a long time due to the insufficient river sediment contribution (Nguyen, 1996; Ton et al., 1996). The tidal flats in Kim Son receive the sediments from the Day River, Ninh Co

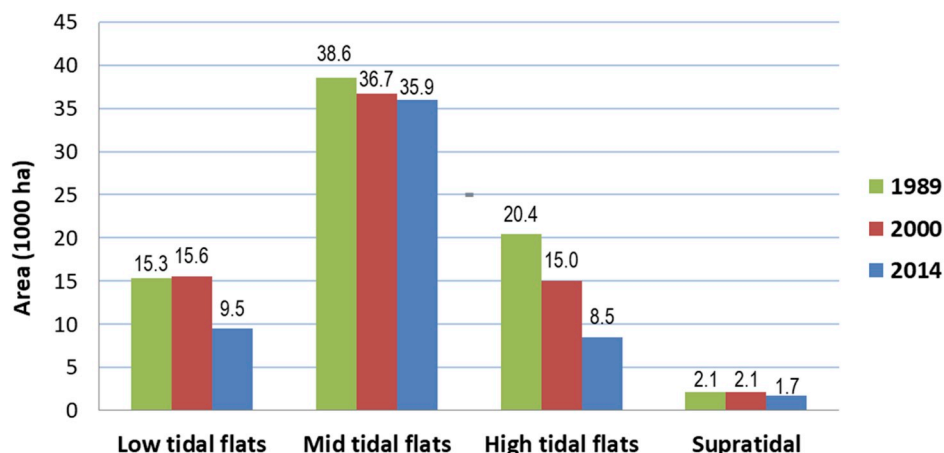


Fig. 8. Area of tidal flat layers in 1989, 2000, 2014.

River, and Len River concentrated in an embayment. Thus, over 25 years, a massive amount of  $26.8 \times 10^6 \text{ m}^3$  of sediments has deposited along the 30 km coast length in Kim Son. Giao Thuy and Tien Hai areas located at both sides of the Red River mouth show a significant deposition with  $35 \times 10^6 \text{ m}^3$  of accreted sediments.

The erosion tends to occur in the northern part of the study area, from Ha Long to Mong Cai. Especially, an amount of  $35.6 \times 10^6 \text{ m}^3$  sediment has exported from the tidal flats over 25 years in Mong Cai. Each year, tidal flats in here lost approximately  $1.4 \times 10^6 \text{ m}^3$  of sediments. Tien Yen is one of the two largest rivers in the northern area, but its sediment discharge is insufficient to compensate for the lost sediments (Nguyen, 2006). Hence, the tidal flats surrounding Dam Ha have a high rate of erosion with a total amount of  $9.2 \times 10^6 \text{ m}^3$  of sediment loss from 1989 to 2014. As the only exception, the coal sediments discharged from coal industries in Cam Pha contribute to the accretion of the tidal flats with  $1.0 \times 10^6 \text{ m}^3$ . Although the erosion processes dramatically occurred in half of the study area, the tidal flats also received  $17.8 \times 10^6 \text{ m}^3$  sediments between 1989 and 2014. When comparing the amount of sediment loss between 11 years (1989–2000) and 14 years (2000–2014), it appears unusual that the erosion rate in 1989–2000 is much more severe than in 2000–2014. In Mong Cai especially, an amount of  $34.2 \times 10^6 \text{ m}^3$  sediment is lost during 1989–2000 but only  $15.5 \times 10^6 \text{ m}^3$  from 2000 to 2014. Besides, tidal flats in Do Son also export a total of  $7.7 \times 10^6 \text{ m}^3$  and  $1.2 \times 10^6 \text{ m}^3$  of sediments during 1989–2000 and 2000–2014, respectively. The amount of sediment transported to the tidal flats can be correlated with the frequency of the tropical cyclones that occurred during the study periods (Table 4).

## 5. Discussions

In term of the waterline method, the accuracy of the DEMs of tidal flats is affected by different error sources coming from the accuracy of extracting waterlines, the reference data of water level or the multi-temporal satellite images in use (Ryu et al., 2008; Xu et al., 2016; Tseng et al., 2017). Although an accuracy assessment is implemented for the constructed DEM, it also faces many issues. The difference between the reference data and the elevation of DEMs may come from the instrument in use, the measuring performance, the accuracy of DEM, or the variation of tidal flats in the duration between DEM constructed in 2014 and field measurement in 2015. As seen in Fig. 6, there is a slightly wavy form of the curves in the middle tidal flats that may be mentioned as a systematic error. The errors caused by the surveying method or instruments in the field measurement can be ignored because they were well tested before the experiment. The change of tidal flats during the period between the field measurement and DEM constructed is usually random at a large scale within a year from 2014 to 2015. The only assumption for the systematic error is coming from the accuracy of

waterlines used to construct DEM 2014. The maximum errors are observed at the elevations of around 1.3 m and 1.7 m (Fig. 6C and 6D). Thus the waterlines at these elevations may be assigned with the uncertain water levels, which are not clearly denoted in the SHOM model. Nevertheless, the error of the DEMs estimated from field measurement data is the composition error from various sources, and it is mentioned as the general accuracy of the constructed DEMs. In this section, we discuss more factors affecting the accuracy of the DEMs constructed by the waterline method.

The precision of the waterline extraction depends on the spectral bands or band ratios, which best represent the contrast between water and exposed tidal flats. Spectral reflectance of tidal flat surfaces and near-shore shallow waters can be measured in the field to determine the suitable spectral band for extracting the waterlines (Lodhi et al., 1997). However, it is difficult to apply this method at large scale because of the rapid variation of suspended sediments in near-shore water. In this study, the comparison between the testing waterlines and a reference waterline for each coastal environment provides a confident solution to determine the suitable spectral band or band ratio for accurately extracting waterlines on satellite images. Thus, this approach should be widely applied for other satellite data as well as other study areas, especially for a specific environment such as the coal tidal flat. The critical criteria for this approach are similar conditions (water level, tidal stage, the turbidity of the shallow coastal water, meteorological conditions) between the reference images and testing images or better if these images are acquired at the same time.

The accuracy of the waterlines also depends on the precision of defining thresholds, which change significantly according to seasonal variations and to the location of the tidal flats (Table 2). For this reason, the implementation of an automatic threshold detection at a large scale is not a promising approach. The thresholds should be defined in several coastal sections corresponding to the different environments. The tidal stage at the acquisition time of satellite images also strongly affects the accuracy of thresholds (Ryu et al., 2008). During the ebb tide, saltwater is retreating from a tidal flat, the surface of which is usually covered by thin remnant water due to the water-saturated sand (silt). The inter-mixing pixels between water-pixels and exposed intertidal-pixels may occur in the images. A slight modification of threshold values may include numerous water pixels or exclude tidal flats with remnant water. In this case, visual digitalization on color composite images can help to produce more accurate waterlines.

Other important factors affecting the accuracy of waterline extraction are the spatial resolution and the registration error of satellite images in use (Kang et al., 2017). Thresholds used to extract waterlines are based on manual visual validation, thus the positional errors of the waterlines are smaller than one-pixel size (30m of Landsat images) (Liu et al., 2012). Also, the RMSE of the geometric registration of Landsat

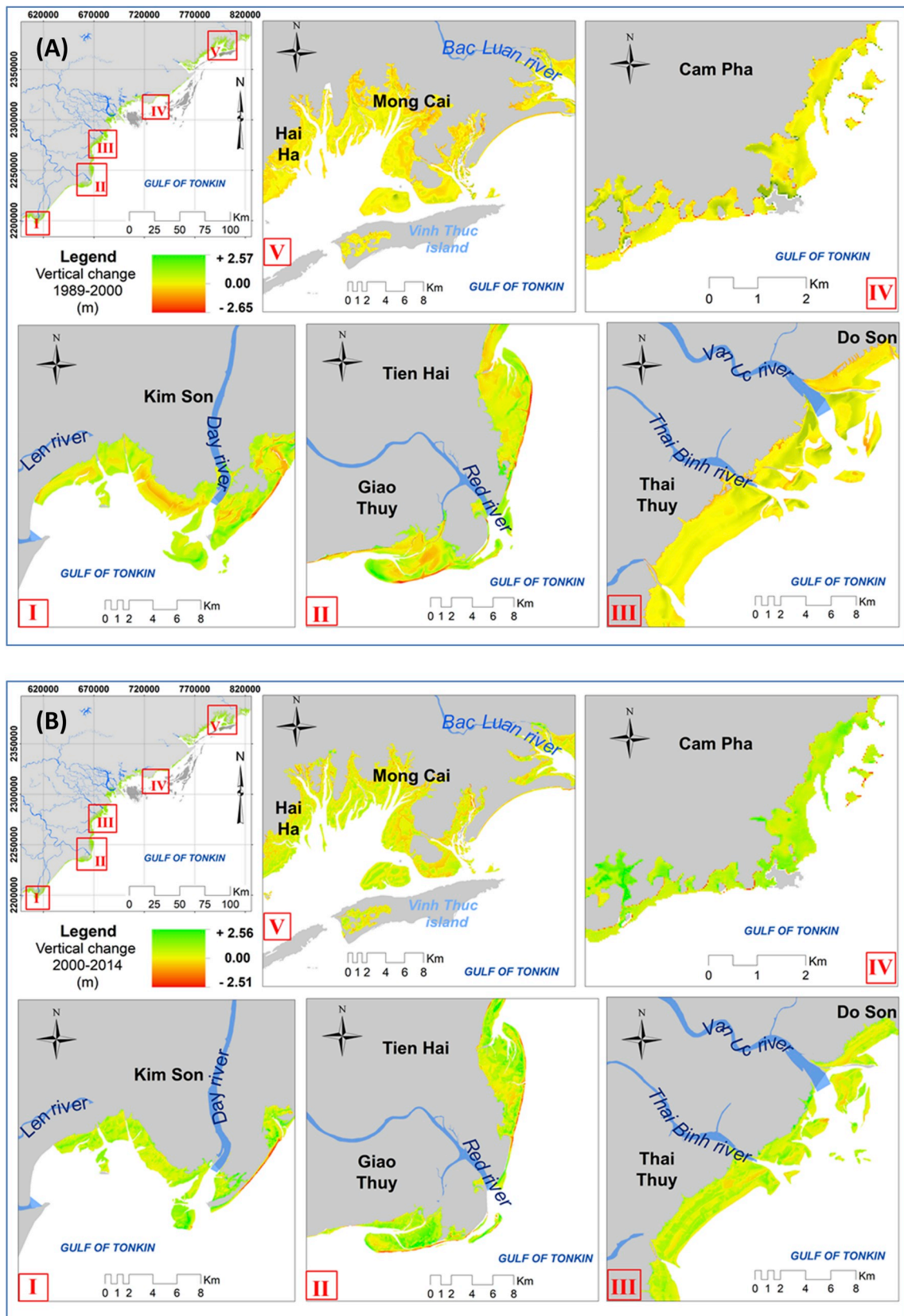


Fig. 9. Vertical change map of tidal flats: (A) during 1989–2000, (B) during 2000–2014.

**Table 3**

The amount of sediment deposition and sediment loss during two periods in the tidal flats.

No	Sections	1989–2000 (10 <sup>6</sup> m <sup>3</sup> )		2000–2014 (10 <sup>6</sup> m <sup>3</sup> )		Sum of sediment transport (10 <sup>6</sup> m <sup>3</sup> )
		Accretion	Erosion	Accretion	Erosion	
1	Kim Son	18.0	-7.4	17.9	-1.7	26.8
2	Hai Hau	0.3	-2.6	0.3	-1.2	-3.2
3	Giao Thuy	11.3	-7.7	13.8	-2.2	15.2
4	Tien hai	13.0	-7.0	17.3	-3.5	19.8
5	Thai Thuy	3.7	-5.5	8.2	-1.0	5.4
6	Do Son	6.4	-7.7	7.8	-1.2	5.3
7	Yen Hung	5.7	-8.6	9.0	-2.5	3.6
8	Ha Long-Hoanh Bo	1.7	-4.2	2.4	-1.5	-1.6
9	Cam Pha	1.2	-1.9	2.1	-0.4	1.0
10	Van Don	0.4	-2.0	1.9	-0.7	-0.4
11	Dam Ha	2.8	-7.6	2.3	-6.7	-9.2
12	Hai Ha	1.8	-7.4	1.8	-5.1	-8.9
13	Mong Cai	6.9	-34.2	7.2	-15.5	-35.6
Total		72.3	-103.4	91.9	-43.0	17.8

images is 12 m (Zanter, 2017). In total, the RMSE of waterline extraction on Landsat images should be 32.3 m because it is the combination of the two error sources. This RSME is smaller than that on the ERS-2 SAR image with an error of 50 m for a spatial resolution of 25 m (Heygster et al., 2010). Tidal flats of the study area have a slope of around 0.1°, and therefore the vertical error corresponding to 32.3 m of positional

waterline error is 0.056 m. The vertical error of the waterline extraction is much smaller than the overall accuracy of constructed DEMs with 0.144 m.

The elevation assigned to waterlines should be seawater levels, which suffer local meteorological factors such as wind, wave, pressure, temperature. However, the effects of factors on water levels have been excluded in both the gauge height and hydrodynamic models. Alternately, the leveling water method can be used to obtain the seawater level with an accuracy of 2 cm (Ryu et al., 2008). However, it could be

**Table 4**

Typhoons with wind speed greater than 89 km/h (Level 10) reached to the study area from 1989 to 2014.

Number	Typhoon name	Date	Wind speed
1	SON TINH	23-Oct-2012	Level 11 (103–117 km/h)
2	NESAT	30-Sep-2011	Level 10 (89–102 km/h)
3	CON SON	12-Jul-2010	Level 11 (103–117 km/h)
4	DAMREY	19-Sep-2005	Level 12 (118–133 km/h)
5	WASHY	28-Jul-2005	Level 10 (89–102 km/h)
6	KROVANH	20-Aug-2003	Level 11 (103–117 km/h)
7	ZITA	20-Aug-1997	Level 11 (103–117 km/h)
8	NIKI	18-Aug-1996	Level 11 (103–117 km/h)
9	FRANKIE	21-Jul-1996	Level 11 (103–117 km/h)
10	HARY	25-Jul-1994	Level 10 (89–102 km/h)
11	LEWIS	7-Jul-1993	Level 10 (89–102 km/h)
12	CHUSK	24-Jun-1992	Level 10 (89–102 km/h)
13	ZEKE	10-Jul-1991	Level 10 (89–102 km/h)
14	ED	11-Sep-1990	Level 10 (89–102 km/h)
15	IRVING	20-Jul-1989	Level 11 (103–117 km/h)
16	DOT	5-Jun-1989	Level 10 (89–102 km/h)

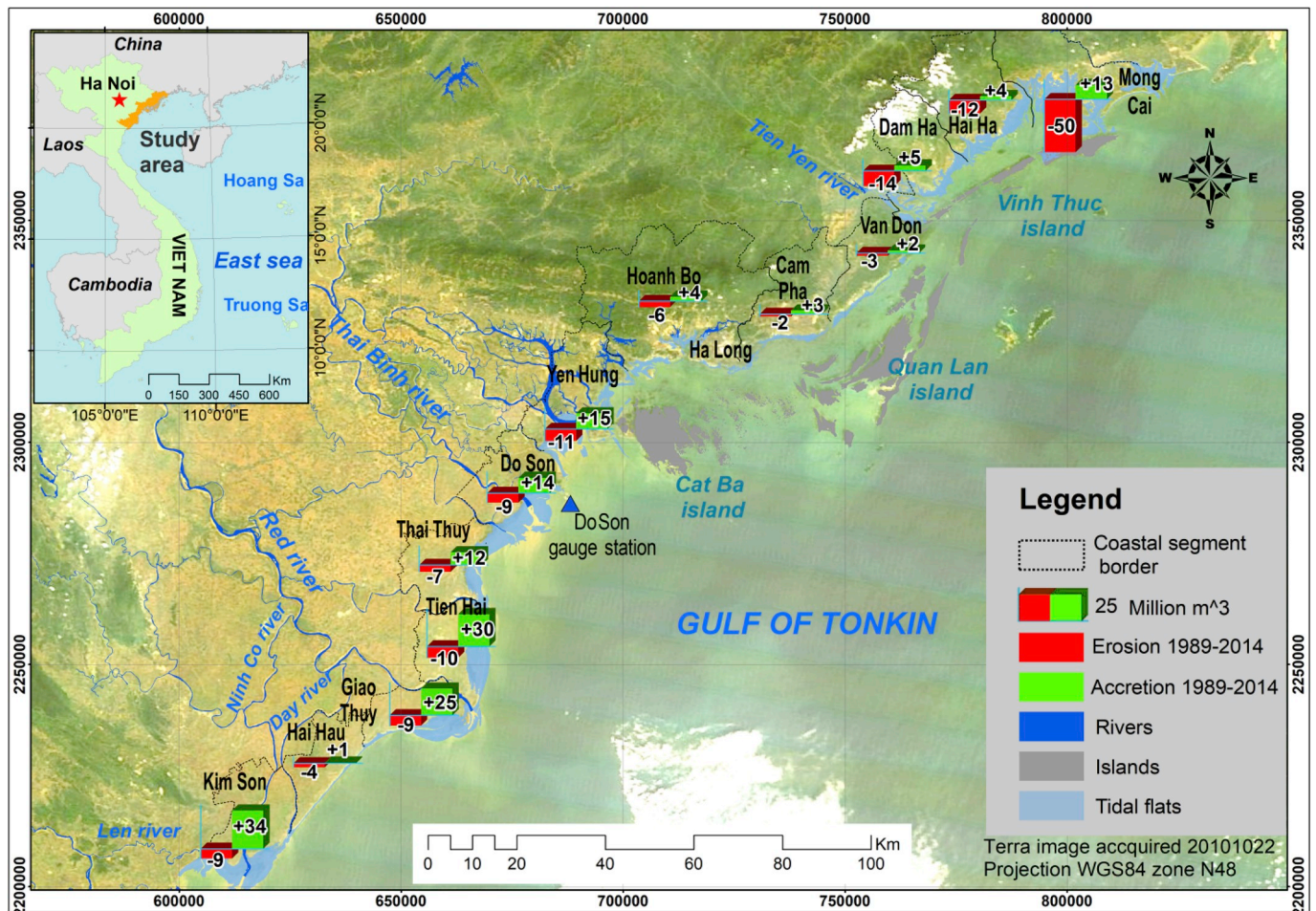


**Fig. 10.** The amount of sediment loss (negative values) and sediment deposition (positive values) in the tidal flat during the period 1989–2014.

impossible to apply the leveling method in the past, and missing data are a common occurrence at the gauge station in the study area. Hence using water levels with the error of 5 cm predicted from the SHOM model is an acceptable solution. This error contributes to the accuracy of DEMs; therefore, the accuracy of tidal flat DEMs in this study is  $0.144 \pm 0.05$  m. Overall, this accuracy agrees with the results of Mason et al. (1997), Ryu et al. (2008), or Kang et al. (2017), who constructed DEMs with a vertical accuracy of 0.14 m, 0.109 m, and 0.182 m, respectively. Consequently, tidal flat DEMs with the vertical accuracy of  $0.144 \pm 0.05$  m are acceptable, reliable, and unique data for quantifying the sediment transport in this study area.

The diurnal tidal wave tends to propagate southward due to the Coriolis forcing (Nguyen et al., 2014), which slightly causes the variation of water level at near-shore from the North to the South of the study area in both amplitude and phase. In this study, we used the tide data referenced at the Hondau station, located in the middle of the study area, to minimize the effect of the diurnal propagating tide on the accuracy of the DEMs. Moreover, this systematic error integrated into a DEM is negligible by subtracting two DEMs from each other to calculate the sediment transport. Still, somehow, a tidal propagation model should be used to estimate the water level for each location in a large study area. This issue may be deeply investigated in further study.

The density of waterlines and the duration of satellite image acquisition are also important factors affecting the accuracy of DEMs (Kang et al., 2017). There is no study figuring out how many waterlines are sufficient. However, it was recommended that the number of waterlines should be as much as possible to well represent the gradual variation of the tidal flat morphology (Ryu et al., 2008; Tseng et al., 2017). Even though the number of satellite images may be sufficiently collected, they should be acquired in a short duration to minimize the effect of the tidal flat change on the accuracy of DEMs. However, it is a big challenge to meet this demand perfectly in tropical regions. The tropical monsoon climate generally coincides with extensive cloud cover that limits the number of usable optical images. Thus, the time span of satellite image acquisition must be lengthened. For this reason, it is difficult to investigate tidal flat changes in such a short term as a monthly or seasonal variation. The use of radar satellite data as the Sentinel 1 constellation or TerraSAR-X (Heygster et al., 2010; Stefan and Susanne, 2015; Adolph et al., 2018) may be a good solution to compensate the gap of optical satellite data. The waterline method applies for multi-satellite image sources may face with the heterogeneity of the accuracy of DEMs due to the discrete spatial resolution and the different types of data.

Tidal flats are commonly zoned into high tidal flats ranged from mean high water neap (MHWN) to mean high water spring (MHWS), mid tidal flats from mean low water neap (MLWN) to MHWN, and low tidal flats from mean low water spring (MLWS) to MLWN. This zonation is based on the sediment distribution and the dominant processes of sedimentation, which form the morphology of tidal flats (Klein, 1985). As seen in Fig. 7C, MHWS and MHWN are defined relatively the same at around 2.96 m, and MLWN is similar to MLWS at approximate 0.89 m. Thus, the zoning method proposed by Klein (1985) does not fit with the tidal flat morphology in the study area. Friedrichs (2011) also recognized that this partitioning method of tidal flats did not always correspond to sharp morphological or sedimentological boundaries. In this study, we emphasize the marked distinctions in the slope of tidal flats, which are relatively defined on the elevation profiles of tidal flats (Fig. 7A). Also, the higher elevation frequency refers to the planar surface (Fig. 7B). The critical elevation at which the frequency changes, illustrates the sudden variation of the bed slope. Eisma (1998) denoted that a zonation of tidal flats was usually related to the duration of submergence, and the subdivision method of all tidal flats was not made in the same ways. In this study, the relative values defined in elevation profiles and elevation frequency are compared to the tidal regime (Fig. 7C) to precise the elevation marks for zoning tidal flats. The correlation between these three components proves that this approach is correct, and it is a new finding to subdivide tidal flats. This subdivision

approach should be further applied in other tidal regions for future studies. Indeed, the morphological analysis of tidal flats must be based on an accurate DEM.

This study provided reliable evidence of the changes in tidal flats in both spatial and temporal dimensions as well. Tidal flats in the north of the study area from Hoanh Bo to Mong Cai tends to be eroded, but a predominant deposition process is found in the south from Kim Son to Yen Hung (Hoa, 2001; Lefebvre et al., 2012). This study discovers an unusual rate of erosion. The total amount of sediment lost during 11 years from 1989 to 2000 with  $103.4 \times 10^6 \text{ m}^3$  is double than that of  $43.0 \times 10^6 \text{ m}^3$  during 14 years of the period 2000–2014 (Table 3). Conventionally, sediments suspended or accumulated in an intertidal area are controlled by main factors: the tide, the wind, the waves, the density-driven circulation, and the drainage process (Hir et al., 2000). The circular processes of sediment transportation are relatively stable during the fair weather in a year (Yang et al., 2003). However, sediments in the un-vegetated tidal flats are extremely driven seaward during storms because of the surge wave energy felt at the seabed, which speeds up the rate of erosion (Christie et al., 1999; Hir et al., 2000; Yang et al., 2003). The study area is located in the western Pacific, which suffers a high frequency of tropical cyclones. As counted from 1989 to 2014, 39 tropical cyclones with a wind speed of greater than 39 km/h directly made landfall to the study area. In these phenomena, 10 of 19 cases occurred during the period 1989–2000 with a wind speed greater than 89 km/h. This wind speed was also the case for 6 of 20 events during the period 2000–2014 (Table 4). The almost double frequency of severe tropical storms might cause more dramatic erosion in the period 1989–2000 than that in the period 2000–2014 (Table 3). The rate of tropical cyclones directly affecting the magnitude of tidal flat erosion is, for the first time, illustrated using the waterline method on the northern coast of Vietnam.

## 6. Conclusions

The morphology and the quantitative variation of tidal flats along the northern coast of Vietnam were firstly, successfully investigated in this study by analyzing the differences between DEMs constructed in 1989, 2000, and 2014 achieved from the waterline method. This study develops an optimal waterline method using the combination of band ratio Green/MIR and NDWI index with multiple thresholds for waterline extraction to overcome the challenges coming from the heterogeneity of tidal flats of the study area. The experiment proved that the tidal flats in the study area could be subdivided into three parts: high tidal flat, mid tidal flat, and low tidal flat based on the slope, elevation frequency, and critical marks of tide regime. Tidal flats in the north of the study area (Hai Ha, Mong Cai) are severely eroded with the rate of sediment loss of  $1.5 \times 10^6 \text{ m}^3/\text{year}$ . Conversely, tidal flats in the south (Giao Thuy, Kim Son) are predominated by high accretion rates, especially the area surrounding river mouths. The sediment loss during 11 years (1989–2000) is much more serious than 14 years of period 2000–2014 that can be explained by the double frequency of severe tropical storms affecting the study area from 1989 to 2000. The topographical data, the trend of tidal flat erosion and deposition are valuable data for such activities as coastal conservation and coastal planning. Furthermore, the amount of sediment import, export in tidal flats obtained from this study provided confident data to calibrate and validate the numerical simulation of sediment transport and coastal evolution in the long term.

The key technique used in this study is the approach to define the appropriate spectral bands or band ratios to determine waterlines on satellite images corresponding to specific coastal environments. This study concluded that the ratio of Green and Middle infrared (MIR) band is the potential solution for determining waterlines in such a coastal tidal flat as in Cam Pha. The NDWI index is suitable for the waterline extraction in the other coastal regions of the study area. Besides, the use of a series of thresholds to extract waterlines for different coastal sections is also a significant point of the experiment. These techniques can

be widely applied to other tidal flats at large scale. The accuracy of DEMs constructed from the waterline method is influenced by various factors in which tidal flat change during the period of satellite image acquisitions is an important one. The increasing number of satellite sources (both optical and radar images) and the development of cloud computing infrastructure improve the accuracy of tidal flat DEM as well as minimize the time to assess, process satellite data that will be employed in future works.

### Declaration of competing interest

The study with the title “An optimal waterline approach for studying tidal flat morphological changes using remote sensing data: a case of the northern coast of Vietnam.” is implemented with the agreements of all authors as well as the corresponding institutions. Hence, there is no conflict of interest in this works.

### CRediT authorship contribution statement

**Si Son Tong:** Writing - original draft, Conceptualization. **Jean Paul Deroin:** Supervision, Funding acquisition. **Thi Lan Pham:** Methodology, Visualization.

### Acknowledgment

This study is implemented in the GEGENAA laboratory, funded by the cooperation between University of Science and Technology of Hanoi (USTH) and Université de Reims Champagne-Ardenne. We express heartfelt thanks to these valuable supports. We thank also to colleagues in Space Technology Institute, VAST who give us the advantage experiences in processing satellite images. We thank the anonymous reviewers for their very constructive reviews.

### Appendix A. Supplementary data

Supplementary data related to this article can be found at <https://doi.org/10.1016/j.ecss.2020.106613>.

### References

- Adolph, W., Farke, H., Lehner, S., Ehlers, M., 2018. Remote sensing intertidal flats with TerraSAR-X. A SAR perspective of the structural elements of a tidal basin for monitoring the Wadden sea. *Rem. Sens.* 10 (7), 1085.
- Bell, P.S., Bird, C.O., Plater, A.J., 2016. A temporal waterline approach to mapping intertidal areas using X-band marine radar. *Coast Eng.* 107, 84–101.
- Bhargava, D.S., Mariam, D.W., 1991. Effects of suspended particle size and concentration on reflectance measurement. *Photogramm. Eng. Rem. Sens.* 57, 19–529.
- Christie, M.C., Dyer, K.R., Turner, P., 1999. Sediment flux and bed level measurements from a macro tidal mudflat. *Estuar. Coast Shelf Sci.* 49, 667–688.
- Department of the Interior, 2016. Landsat 4-7 Climate Data Record (CDR) Surface Reflectance, p. 27, Version 6.4.
- Deroin, J.-P., 2012. Combining ALOS and ERS-2 SAR data for the characterization of tidal flats. A case study from the Baie des Veys, Normandy, France. *Int. J. Appl. Earth Obs. Geoinf.* 18, 183–194.
- Deroin, J.-P., Shimada, M., 2010. The importance of local mean time in remote sensing for mapping mega tidal zones. *Compt. Rendus Geosci.* 342 (1), 11–18.
- Eisma, D., 1998. *Intertidal Deposits: River Mouths, Tidal Flats, and Coastal Lagoons*. CRC Press, Boca Raton.
- Flemming, B.W., 2002. Geographic distribution of muddy coasts Muddy coast of the world. In: Healy, T., Wang, Y., Healy, J.-A. (Eds.), *Processes, Deposits, and Function*. Elsevier Science B.V., Amsterdam, The Netherlands, pp. 99–203.
- Friedrichs, C.T., 2011. *Tidal Flat Morphodynamics; A Synthesis*. Elsevier Inc, pp. 137–170.
- Guariglia, A., Buonamassa, A., Losurdo, A., Saladino, R., Trivigno, M.L., Zaccagnino, A., Colangelo, A., 2006. A multisource approach for coastline mapping and identification of shoreline changes. *Ann. Geophys.* 49 (1), 295–304.
- Heygster, G., Dannenberg, J., Notholt, J., 2010. Topographic mapping of the German tidal flats analyzing SAR images with the waterline method. *IEEE Trans. Geosci. Rem. Sens.* 48 (3), 1019–1030.
- Hir, P.L., Roberts, W., Cazaillet, O., Christie, M., Bassoullet, P., Bacher, C., 2000. Characterization of intertidal flat hydrodynamics. *Continent. Shelf Res.* 20, 1433–1459.
- Hoa, M.H., 2001. *Morphological Dynamics the Estuary of the Delta in North Vietnam Serves the Rational Use of Natural Resources and the Environment in the Estuary Area*. Doctor. Ha Noi university of science, Vietnam national university.
- Jackson, J.A., Bates, R.L., 1997. *Glossary of Geology*. American Geological Institute.
- Kang, Y., Ding, X., Xu, F., Zhang, C., Ge, X., 2017. Topographic mapping on large-scale tidal flats with an iterative approach on the waterline method. *Estuar. Coast Shelf Sci.* 190, 11–22.
- Klein, G.d.V., 1985. Intertidal flats and intertidal sand bodies. *Coast Sediment Environ.* 187–224.
- Koopmans, B.N., Wang, Y., 1994. Satellite radar data for topographic mapping of the tidal flats in the Wadden Sea, The Netherlands. In: *Proc. Second Thematic Conference on Remote Sensing for Marine and Coastal Environments*. New Orleans.
- Lee, K.-S., Kim, T.-H., 2004. Topographic relief mapping on Inter-tidal mudflat in Kyongki bay area using infrared bands of multi-temporal Landsat TM data. *Kor. J. Remote Sens.* 20 (3), 163–173.
- Lee, K.-S., Kim, T.-H., Yun, Y.-S., Shin, S.-M., 2001. Spectral characteristics of shallow turbid water near the shoreline on inter-tidal flat. *Kor. J. Remote Sens.* 17 (2), 131–139.
- Lefebvre, J.-P., Sylvain, O., Vu, D.V., Arfi, R., Panché, J.-Y., Mari, X., Chu, V.T., Torrétou, J.-P., 2012. Seasonal variability of cohesive sediment aggregation in the Bach Dang–Cam estuary, Haiphong (Vietnam). *Geo Mar. Lett.* 32 (2), 103–121.
- Liu, Y., Li, M., Cheng, L., Li, F., Chen, K., 2012. Topographic mapping of offshore sandbank tidal flats using the waterline detection method: a case study on the Dongsha Sandbank of Jiangsu Radial Tidal Sand Ridges, China. *Mar. Geodes.* 35, 362–378.
- Lodhi, M.A., Rundquist, D.C., Han, L., Kuzila, M.S., 1997. The potential for remote sensing of loess soils suspended in surface water. *J. Am. Water Resour. Assoc.* 33 (1), 111–127.
- Lohani, B., Mason, D.C., 1999. Construction of a digital elevation model of the holderness coast using the waterline method and airborne thematic mapper data. *Int. J. Rem. Sens.* 20 (3), 593–607.
- Mackinnon, J., Verkuil, Y.I., Murray, N., 2012. IUCN situation analysis on East and Southeast Asian intertidal habitats, with particular reference to the Yellow Sea (including the Bohai Sea). In: *Occasional Paper of the IUCN Species Survival Commission No. 47*, p. 70.
- Mason, D.C., Davenport, I.J., Robinson, G.J., Flather, R.A., McCartney, B.S., 1995. Construction of an inter-tidal digital elevation model by the ‘water-line’ method. *Geophys. Res. Lett.* 22 (23), 3187–3190.
- Mason, D.C., Hill, D., Davenport, I.J., Flather, R., Robinson, G.J., 1997. Improving intertidal digital elevation models constructed by the waterline technique. In: *ERS Symposium on Space at the Service of Our Environment No3*, Florence, ITALIE.
- Mason, D.C., Marani, M., Belluco, E., Feola, A., Ferrari, S., Katzenbeisser, R., Lohani, B., Menenti, M., Paterson, D.M., Scott, T.R., Vardy, S., Wang, C., Wang, H.-J., 2005. Lidar mapping of tidal marshes for ecogeomorphological modeling in the tide project. In: *The Eighth International Conference on Remote Sensing for Marine and Coastal Environments*. Nova Scotia, Halifax, pp. 17–19.
- McFeeters, S.K., 1996. The use of the Normalized Difference Water Index (NDWI) in the delineation of open water features. *Int. J. Rem. Sens.* 17, 1425–1432.
- Murray, N.J., Phinn, S.R., Clemens, R.S., Roelfsema, C.M., Fuller, R.A., 2012. Continental scale mapping of tidal flats across East Asia using the Landsat archive. *Rem. Sens.* 4 (12), 3417–3426.
- Nguyen, D.C., 1996. Investigation of tidal flats along the coast and nearshore islands in NorthEast Vietnam. In: *National investigation project*. Hai Phong.
- Nguyen, V.T., Tran, D.T., Saito, Y., Gouramanis, C., 2013. Monitoring coastline change in the Red River delta using remotely sensed data. *J. Mar. Sci. Technol.* 13 (2).
- Nguyen, V.C., 2006. Tidal flats in the northern coast of Vietnam. *Vietnam Academy of Science and Technology*, Hanoi.
- Nguyen, N.M., Patrick, M., Florent, L., Sylvain, O., Gildas, C., Damien, A., Dinh, V.U., 2014. Tidal characteristics of the gulf of Tonkin. *Continent. Shelf Res.* 91, 37–56.
- Niya, A.K., Alesheikh, A.A., Soltanpor, M., Kheirkhahzarkesh, M.M., 2013. Shoreline change mapping using remote sensing and GIS. *Int. J. Rem. Sens. Appl.* 3 (3).
- Pham, T.L., Pham, V.C., Tong, S.S., 2010. Using remote sensing and GIS to assess mangrove cover change in the coastal zone of Thai Binh province. In: *The 19th Scientific Conference*. University of Mining and Geology, Ha Noi, pp. 71–78.
- Ryu, J.-H., Kim, C.-H., Lee, Y.-K., Won, J.-S., Chun, S.-S., Lee, S., 2008. Detecting the intertidal morphologic change using satellite data. *Estuar. Coast Shelf Sci.* 78 (4), 623–632.
- Sibson, R., 1981. A brief description of natural neighbor interpolation. *Interpret. Multivariate Data* 21, 21–36.
- Stefan, W., Susanne, L., 2015. Automated waterline detection in the Wadden sea using high-resolution TerraSAR-X images. *J. Sensors* 1–6, 2015.
- Ton, T.V., Kant, G., Nguyen, N.H., Pruszak, Z., 1996. Sea dike erosion and coastal retreat at Nam Ha province, Vietnam. *Coast Eng.* 218, 2820–2828.
- Tong, S.S., Pham, T.L., Gunasekara, K., Nguyen, T.N., Deroin, J.-P., 2014. Monitoring coastal morphological changes using remote sensing and GIS in the Red River delta area, Vietnam. *Photo Interpret. Eur. J. Appl. Remote Sens.* 50, 36–63.
- Tran, V.D., Tran, D.T., Nguyen, V.T., 2003. Monitoring coastal erosion in Red River Delta, Vietnam – a contribution from remote sensing data. *Asian J. Geoinf.* 3 (3), 73–79.
- Tseng, K.-H., Kuo, C.-Y., Lin, T.-H., Huang, Z.-C., Lin, Y.-C., Liao, W.-H., Chen, C.-F., 2017. Reconstruction of time-varying tidal flat topography using optical remote sensing imageries. *ISPRS J. Photogrammetry Remote Sens.* 131, 92–103.
- Wang, Y., Liu, Y., Jin, S., Sun, C., Wei, X., 2019. Evolution of the topography of tidal flats and sandbanks along the Jiangsu coast from 1973 to 2016 observed from satellites. *ISPRS J. Photogrammetry Remote Sens.* 150, 27–43.

- Won, J.-S., Kim, S.-W., 2003. "ERS SAR Interferometry for Tidal Flat DEM." Fringe 2003 Workshop. Frascati, Italy.
- Xie, Y., Zhang, X., Ding, X., Liu, S., Zhang, C., 2011. Salt-marsh geomorphological patterns analysis based on remote sensing images and lidar-derived digital elevation model: a case study of Xiaoyangkou, Jiangsu. In: International Symposium on Lidar and Radar Mapping 2011: Technologies and Applications.
- Xu, Z., Kim, D.-j., Kim, S.H., Cho, Y.-K., Lee, S.-G., 2016. Estimation of seasonal topographic variation in tidal flats using waterline method: a case study in Gomso and Hampyeong Bay, South Korea. *Estuar. Coast Shelf Sci.* 183, 213–220.
- Yang, S.L., Friedrichs, C.T., Shi, Z., Ding, P.X., Zhu, J., Zhao, Q.Y., 2003. Morphological response of tidal marshes, flats, and channels of the outer Yangtze River mouth to a major storm. *Estuaries* 26, 1416–1425.
- Zanter, K., 2017. Landsat Collection 1 Level 1 Product Definition. Department of the Interior U.S. Geological Survey. LSDS-1656, Version 10.